Journal Pre-proof

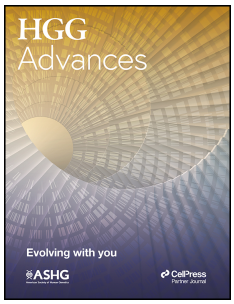

Expanding the *ABCA2*-associated neurodevelopmental phenotype

Kaisa T. Oja, Karit Reinson, Mihkel Ilisson, Daima Örd, Monica H. Wojcik, Eleanor G. Seaby, Bryan M. Wittmann, Adam D. Kennedy, Karen DeBalsi, Christiane Zweier, Georgia Vasileiou, Issam A. Alkhawaja, Thomas Wirth, Steffen Syrbe, Konrad Platzer, Suad Alyamani, Fowzan S. Alkuraya, David Ros-Pardo, Iñigo Marcos-Alcalde, Paulino Gómez-Puertas, Marie Vidailhet, Ke Su, Shaohua Fan, Yu Ma, Yi Wang, Alessandra Renieri, Anna Maria Pinto, Farah Almadhoun, Andrea K. Petersen, Kari Magnussen, Olaf Bodamer, Talal Alanzi, Sarar Mohamed, Hadeel Alrabee, Bader Alhaddad, Khadijah Bakur, Nicole Fleischer, Amber Begtrup, Tõnis Örd, Sander Pajusalu, Katrin Õunap

PII: S2666-2477(26)00078-3

DOI: https://doi.org/10.1016/j.xhgg.2026.100638

Reference: XHGG 100638

To appear in: *Human Genetics and Genomics Advances*

Received Date: 19 February 2026

Accepted Date: 23 June 2026

Please cite this article as: Oja KT, Reinson K, Ilisson M, Örd D, Wojcik MH, Seaby EG, Wittmann BM, Kennedy AD, DeBalsi K, Zweier C, Vasileiou G, Alkhawaja IA, Wirth T, Syrbe S, Platzer K, Alyamani S, Alkuraya FS, Ros-Pardo D, Marcos-Alcalde I, Gómez-Puertas P, Vidailhet M, Su K, Fan S, Ma Y, Wang Y, Renieri A, Maria Pinto A, Almadhoun F, Petersen AK, Magnussen K, Bodamer O, Alanzi T, Mohamed S, Alrabee H, Alhaddad B, Bakur K, Fleischer N, Begtrup A, Örd T, Pajusalu S, Õunap K, Expanding the *ABCA2*-associated neurodevelopmental phenotype, *Human Genetics and Genomics Advances* (2026), doi: https://doi.org/10.1016/j.xhgg.2026.100638.

Expanding the *ABCA2*-associated neurodevelopmental phenotype

Kaisa T. Oja,[1,2] Karit Reinson,[1,2] Mihkel Ilisson,[1,2] Daima Örd,[3] Monica H. Wojcik,[4,5] Eleanor G. Seaby,[5,6] Bryan M. Wittmann,[7] Adam D. Kennedy,[7] Karen DeBalsi,[7] Christiane Zweier,[8,9] Georgia Vasileiou,[9] Issam A. Alkhawaja,[10] Thomas Wirth,[11] Steffen Syrbe,[12] Konrad Platzer,[13] Suad Alyamani,[14] Fowzan S. Alkuraya,[14] David Ros-Pardo,[15] Iñigo Marcos-Alcalde,[15] Paulino Gómez-Puertas,[15] Marie Vidailhet,[16] Ke Su,[17,18] Shaohua Fan,[17] Yu Ma,[19] Yi Wang,[19,20] Alessandra Renieri,[21,22,23] Anna Maria Pinto,[23] Farah Almadhoun,[21] Andrea K. Petersen,[24] Kari Magnussen,[24] Olaf Bodamer,[4] Talal Alanzi,[25] Sarar Mohamed,[26,27,28] Hadeel Alrabee,[26,29] Bader Alhaddad,[30] Khadijah Bakur,[30] Nicole Fleischer,[31] Amber Begtrup,[32] Tõnis Örd,[3] Sander Pajusalu,[1,2] Katrin Õunap*[1,2,33]

Affiliations

[1] Genetics and Personalized Medicine Clinic, Tartu University Hospital, Tartu, 50406, Estonia

[2] Department of Genetics and Personalized Medicine, Institute of Clinical Medicine, University of Tartu, Tartu, 50406, Estonia

[3] Institute of Genomics, University of Tartu, Tartu, 51010, Estonia

[4] Division of Genetics and Genomics, Boston Children's Hospital, Boston, MA, USA

[5] Program in Medical and Population Genetics, Broad Institute of MIT and Harvard, Cambridge, MA, USA

[6] Department of Paediatrics, Imperial College London, London, UK

[7] Metabolon, 617 Davis Drive, Suite 100, Morrisville, NC, USA

[8] Department of Human Genetics, Inselspital Bern, University of Bern, Bern, Switzerland

[9] Institute of Human Genetics, Universitätsklinikum Erlangen, Friedrich-Alexander-Universität Erlangen-Nürnberg, Erlangen, Germany

[10] Albashir Hospital, Amman, Jordan

[11] Strasbourg University Hospital, Strasbourg, France

[12] Heidelberg University, Medical Faculty of Heidelberg, Center for Child and Adolescent Medicine, Clinic 1, Division of Pediatric Epileptology, Heidelberg, Germany

[13] Institute of Human Genetics, University of Leipzig Medical Center, Leipzig, Germany

[14] King Faisal Specialist Hospital and Research Centre, Riyadh, Saudi Arabia

[15] Molecular Modeling Group, Centro de Biología Molecular Severo Ochoa, CBMSO (CSIC-UAM), E-28049 Madrid, Spain

[16] Sorbonne University, Department of Neurology, Salpetriere Hospital, APHP, Paris Brain Institute (ICM) Paris, France

[17] State Key Laboratory of Genetic Engineering, Human Phenome Institute, School of Life Sciences, Fudan University, Shanghai, 200438, China

[18] MOE Key Laboratory of Contemporary Anthropology, Department of Anthropology and Human Genetics, School of Life Sciences, Fudan University, Shanghai, 200433, China

[19] Division of Neurology, Children's Hospital of Fudan University, No. 399 Wanyuan Road, Shanghai, 201102, China

[20] Institute of Brain Science, Fudan University, 138, Yi Xue Yuan Rd,Shanghai, 200032, China

[21] Medical Genetics, University of Siena, 53100 Siena, Italy

[22] Med Biotech Hub and Competence Center, Department of Medical Biotechnologies, University of Siena, 53100 Siena, Italy

[23] Genetica Medica, Azienda Ospedaliero-Universitaria Senese, 53100 Siena, Italy

[24] Randall Children's Hospital at Legacy Emanuel Medical Center, Portland, OR 97227, USA

[25] Women and Children's Health Department, Johns Hopkins Aramco Healthcare Center, Dhahran, Saudi Arabia

[26] Department of Genetics and Metabolic Medicine, Prince Sultan Military Medical City, Riyadh, Saudi Arabia

[27] Department of Pediatrics, College of Medicine, Alfaisal University, Riyadh, Saudi Arabia

[28] Faculty of Medicine, National University, Khartoum, Sudan

[29] King Abdullah Medical Complex, Jeddah, Saudi Arabia

[30] Lifera Omics, Riyadh, Saudi Arabia

[31] FDNA Inc., Boston, Massachusetts, USA

[32] GeneDx, 207 Perry Parkway, Gaithersburg, MD, USA

[33] lead contact

Corresponding author information:

Katrin Õunap ORCID ID:0000-0002-4594-6364

Correspondence and requests for materials should be addressed to Prof. Katrin Õunap, Department of Genetics and Personalized Medicine, Institute of Clinical Medicine, University of Tartu, Tartu, Estonia.

*Email address: katrin.ounap@kliinikum.ee

ABSTRACT

The ATP-binding cassette subfamily A member 2 (ABCA2) gene encodes an ABC transporter protein. Biallelic loss-of-function variants in *ABCA2* have been associated with an intellectual disability disorder. We aimed to delineate the phenotypic spectrum of individuals with monoallelic (MV) or biallelic (BV) variants in the *ABCA2* gene. We collected clinical data via questionnaires and literature review. The ABCA2 protein was constructed using homology modeling. Untargeted plasma metabolomics was performed at Metabolon Inc. A docetaxel toxicity cell culture model system was used to study the effect of plasmid-encoded ABCA2 and four ABCA2 variants (p.Asp615Glu, p.Phe754Ser, p.Ile786del, p.Arg926Trp) on cell viability. Seventeen individuals with seventeen candidate *ABCA2* variants were identified (seven MV, ten BV). Protein modeling predicted a likely significant impact for eight of 13 assessed variants. In cell viability assays, enforced expression of wild type ABCA2 reduced viability in docetaxel-exposed cells. In contrast, none of the four variants affected viability, suggesting a loss or a marked reduction in transporter function. Untargeted metabolomics of three samples from two individuals showed a trend toward lower levels of polyunsaturated acylcarnitines. This study describes 17 individuals with candidate variants in the *ABCA2* gene. The cell viability assays revealed that four variants (p.Asp615Glu, p.Phe754Ser, p.Ile786del, p.Arg926Trp) had an altered ability to function as a transporter compared to wild type ABCA2. Further studies are needed to clarify the pathomechanism of *ABCA2* and the clinical significance of the variants.

Keywords: ABCA2, neurodevelopmental disorder, untargeted metabolomics, cell viability assay

Introduction

The plasma membrane of cells and the membranes of eukaryotic organelles contain ATP-binding cassette (ABC) transporters.[1] The family of ABC transporters comprises energy-dependent transmembrane proteins that actively facilitate the transport of molecules, spanning from simple compounds like sugars and fatty acids to complex ones such as polysaccharides and lipids.[2] Since the discovery of the ABC transporter B1 in 1976[3], at least seven ABC transporter subfamilies with over forty genes have been identified in humans.[4]

The ATP-binding cassette subfamily A member 2 (ABCA2) protein, encoded by the *ABCA2* gene (HGNC:32, MIM: 600047), is composed of conserved ABC transporter domains, specifically two transmembrane (TM) domains and two nucleotide-binding domains with an intervening loop domain.[4] Abca2 was initially identified in embryonic mouse brain tissue.[5] ABCA2 is an endolysosomal membrane protein that mediates cross-membrane transportation of various substances, and it has been implicated in the modulation of sterol, sphingolipid, and cholesterol metabolism.[4,6,7] Abca2 has high expression in brain tissue, and knockout mice display neurological symptoms consistent with aberrant myelination.[8,9] Homozygous loss-of-function variants have been described as the cause of intellectual disability (ID) with poor growth and with or without seizures or ataxia (MIM: 618808) in seven individuals[10–12], and in 2024, a similar phenotype was reported by Inoue et al[13] in an individual with compound heterozygous variants.

This study aimed to further delineate the *ABCA2*-related phenotype. We hypothesized that *ABCA2* pathogenic variants could exhibit both autosomal dominant and recessive inheritance patterns, as has been observed for an increasing number of genes. In 2025, Ezer et al. summarized the characteristics of known genes with multiple inheritance patterns and cautioned geneticists not to discard potential disease-causing variants solely based on inheritance.[14] Pathogenic variants in two other members of the ATP-binding cassette family, *ABCA1* (HGNC:29, MIM: 600046) and *ABCC9* (HGNC:60, MIM: 601439), are known to have different inheritance patterns.[15–17]

We collected clinical, biochemical, and molecular data of 17 patients with mono- or biallelic candidate variants in the *ABCA2* gene. Further analyses were possible in five individuals (three with heterozygous variants and two siblings with a homozygous variant) – cell viability assays with all four variants and untargeted metabolomics analysis in three samples from two of these individuals.

Subjects, material, and methods

Cohort description

The study has been conducted in accordance with the Declaration of Helsinki. Prior to enrolment, informed consent was obtained from the participants in compliance with protocols approved by the institutional review board (IRB) or equivalent ethics committee of each participating institution: Friedrich-Alexander-Universität Erlangen-Nürnberg, Germany (#259_16 Bc); AlBashir Hospital, Jordan; University of Tartu, Estonia [#259/T-2 (16.05.2016), #263/M-16 (17.10.2016), #269/M-18 (17.04.2017), #283/M-10 (18.06.2018), #287/M-15 (19.11.2018), #327/T-3 (19.10.2020), #366/M-6 (15.08.2022), #371/M-13 (21.11.2022)]; University Hospital Heidelberg, Germany; Fudan University, China; University of Siena, Italy; Strasbourg University Hospital, France; King Faisal Specialist Hospital and Research Centre, KSA (RAC# 2121 053); Legacy Emanuel Medical Center, USA; Boston Children's Hospital, USA; Johns Hopkins Aramco Healthcare Center, Saudi Arabia; Alfaisal University, Saudi Arabia.Consent for publication of facial photographs was obtained separately.

We collected data from 17 affected individuals in 15 unrelated families worldwide. International collaboration was established using the Broad seqr[18] and GeneMatcher[19] nodes of the Matchmaker Exchange platform.[20] For all individuals, we asked the clinicians to fill in a questionnaire about birth anomalies, early childhood psychomotor development, brain imaging, laboratory findings, and a current clinical description (Table S1, Supplemental note: case reports). If available, we collected facial photos to supplement the potential dysmorphism descriptions and plasma samples for untargeted metabolomics.

Due to limited resources, a selection of individuals for the cell viability assay had to be made. Based on molecular data, in silico pathogenicity predictions, and the availability of plasma samples for metabolomics, we decided to focus on five persons from four families in our study cohort (individuals 1, 3, 5-7). Individuals 3 and 5 were included because metabolomics data were available; individual 4 was excluded because the metabolomics sample was obtained shortly before the patient's death and was therefore not included in subsequent analyses. Individual 1 was selected as it harbored a de novo heterozygous missense variant with in silico predictions ranging from benign supporting to likely pathogenic, and we hypothesized that additional experimental evidence could help clarify its classification. Individuals 6 and 7 were included to evaluate homozygous variants; as siblings, they provided an opportunity to assess the same variant in two individuals. Moreover, because their variant was an in-frame deletion, fewer in silico predictions were available compared to missense variants. During the preparation of this manuscript, a case was published with a review of the available literature; therefore, we based the layout of Table 1 on the summary by Inoue et al.[13] to facilitate comparison. Additionally, we included the available data from published cases in Tables S1, S2, S3.[10–13]

Molecular analysis

Variants in the *ABCA2* gene were detected by exome sequencing in all individuals. The specifics of molecular analysis platforms and pipelines are provided in Table S3.

We looked at different *in silico* prediction scores, such as CADD[21], REVEL[22], and AlphaMissense[23]; the first two are also included in the meta-score MetaRNN[24]. MetaDome 2.0[25] was used to analyze and visualize whether the missense variants are located in a region intolerant to missense variation in the ABCA2 gene/protein (GENCODE: ENST00000341511.11, RefSeq: NM_001606.5, UniProt: Q9BZC7-3). The automated ACMG classification[26] was generated using the variant data discovery tool Varsome[27] and manually curated to include the inheritance type. The variant nomenclature was checked using VariantValidator[28], and RefSeq NM_001606.5 is used throughout the manuscript. The *in silico* predictions are summarized in Table S2, and the MetaDome visualization is shown in Figure 1.

3D structure of human ATP-binding cassette sub-family A member 2

ABCA2 protein was constructed by homology modeling techniques using the published structures of ABCA1 protein (PDB id: 5XJY)[29] and various states of ABCA4 protein (PDB ids: 7E7I, 7E7O, 7E7Q, 7M1P, and 7M1Q)[30,31]. The model was built using the SWISS-MODEL server (https://swissmodel.expasy.org). The model quality was assessed using standard methods for protein structure evaluation. Overall, the structural quality fell within the acceptable range for homology-based structures. The values obtained were as follows. The MolProbity Score[32] was 3.0 (values of 2.0–3.0 are indicative of average mid-resolution structures; a score of 1.5–2.0 is considered high quality; scores above 3.0 indicate less accurate structures). The QMEANDisCo Global Score[33] was 0.58 ± 0.05 (values of 0.5–0.6 are indicative of reliable models; a score above 0.70 is considered high quality; scores around 0.6 or higher are generally seen as reliable; models with scores below 0.5 are often deemed low quality). The ModFOLD9 global quality score[34] was 0.62 (range between 0 and 1: scores greater than 0.4 generally indicate confident models). Additionally, the obtained model was compared with a model generated using the Alphafold-3 server (https://alphafoldserver.com). The RMSD value difference between the alpha carbon positions in the two models was less than 2.0 Å, with an average pLDDT score[35] for the server model of 70.25 (values of 70–90 indicate a high score). Figures were generated using the Pymol Molecular Graphics System (Schrödinger, LLC, Portland, OR). The protein structure and the positions of ABCA2 variants are shown in Figure 1, and the animated 3D model is in Supplemental Video 1. The model represents the phospholipid-bound state of the protein, and three phospholipid molecules are included in the transmembrane (TM) domain of the model. Two luminal (intralysosomal) asparagine residues (Asn477 and Asn1678) are shown in a glycosylated state as they correspond to two conserved Asn positions of the ABCA4 protein, where their glycosylation has been experimentally determined. The model is based on the Q9BZC7-3 isoform of the protein, as this corresponds to the transcript NM_001606.5 used for describing the genetic variants. The length of this isoform differs by one amino

acid from the canonical Q9BZC7-1 isoform because the Q9BZC7-3 isoform has valine and serine instead of an alanine at positions 54-55.

Untargeted metabolomics

For untargeted metabolomics (including lipidomics) analysis, four mL of EDTA plasma was collected from two individuals (individuals 3 and 5); in individual 3, two samples were obtained at different time points. The collected samples were frozen (-80°C) and shipped out to Metabolon Inc. in the USA, where the untargeted metabolomic profiling test was used for analysis.[36] This Laboratory-Developed Test (LDT), performed in a CLIA-certified laboratory, detects over 800 small molecules (ranging from 50 to 1,500 Daltons in molecular weight). The test uses four different methods of high-performance Ultra Performance Liquid Chromatography (UPLC) instruments paired with Mass Spectrometry (UPLC/ MS).[37] Detected molecules were identified by comparison to a chemical reference library, with unique biochemical entries characterized by accurate molecular mass, including information on any adductation, in source fragmentation, and/or polymerization (typically dimers and trimers) and retention time/index on the chromatography columns. The results were reported as Z-scores and were calculated using a reference cohort of 866 pediatric samples (~50% male and ~50% female). These comparisons were made to provide the most relevant reference ranges for each biochemical, since multiple biochemicals can change in abundance during aging. Individual concentrations were not reported.

Cell viability assays

Plasmids

We designed plasmids which express the protein coding region of ABCA2 transcript 1 (NM_001606.5, protein isoform Q9BZC7-3) (the plasmid was named pCV-ABCA2) or the same coding region containing the disease-associated genetic variation c.1845C>A (the variation in the encoded amino acid sequence is p.Asp615Glu; the plasmid was named pCV-Asp615Glu), c.2261T>C (p.Phe754Ser; plasmid pCV-

Phe754Ser), c.2356_2358del (p.Ile786del; plasmid pCV-Ile786del) or c.2776C>T (p.Arg926Trp; plasmid pCV-Arg926Trp). Myc-tag and Flag-tag were fused to the C-terminus of ABCA2 or its variants encoded by the plasmids, and the proteins are expressed under the control of human cytomegalovirus immediate early enhancer/promoter. A plasmid construct containing a 249-bp DNA segment encoding amino acids 2-83 of E. coli β-galactosidase, instead of *ABCA2* or its variants, was used as a control plasmid (negative control). The plasmids were prepared by VectorBuilder (Chicago, USA). Expression plasmid for Enhanced Yellow Fluorescent Protein (pEYFP) (Clontech) was used as a control for transfection efficiency.

Cultivation of cells

HEK293 cells were maintained in Dulbecco's Modified Eagle Medium (DMEM; 4.5 g/L D-glucose) supplemented with 10% fetal bovine serum (FBS) and 1× penicillin-streptomycin at 37 °C in a 5% CO_2 atmosphere (all medium components from Gibco, Paisley, UK).

Real-Time quantitative PCR (RT-qPCR) and immunoblot analysis

To analyze the expression of plasmid-encoded ABCA2 and its variants, HEK293 cells were seeded onto poly-L-lysine-coated 12-well plates (3.5×10^5 cells per well) and transfected with the corresponding expression constructs using Lipofectamine 3000 Transfection Reagent (Invitrogen) according to the manufacturer's instructions. Cells were collected 40 h post-transfection and analyzed via RT-qPCR and immunoblot to investigate gene expression. In addition, untransfected HEK293 cells treated with docetaxel for 24 h or left untreated were collected to measure mRNA levels. For RT-qPCR analysis, total RNA was extracted from cells using TRIzol (Invitrogen), quantified with the NanoDrop 1000 spectrophotometer (Thermo Scientific), treated with DNase I and reverse-transcribed into cDNA using a FIREScript reverse transcriptase (Solis BioDyne). RT-qPCR was performed as described previously.[38] Control qPCR reactions without a reverse transcription step were performed to confirm the elimination of DNA contamination in RNA samples. The primer pairs used were 5′-CACCTGAAGAACCGGTTTGG-3′ and 5′-AGATGTGCTCCGACTTGAGC-3′ for human ABCA2 mRNA amplification and 5′-TGCACCACCAACTGCTTAGC-3′ and 5′-GGCATGGACTGTGGTCATGAG-3′ for glyceraldehyde-3-phosphate

dehydrogenase (GAPDH) mRNA amplification (used as the endogenous reference for expression level normalization).

For immunoblot analysis, cells were lysed in RIPA buffer (50 mM Tris-HCl pH 8, 150 mM NaCl, 1% NP-40, 0.5% sodium deoxycholate, 0.1% SDS, 10 mM NaF, and complete protease inhibitor cocktail (Roche)). The lysates were incubated on ice for 30 minutes, sonicated using a Bioruptor Plus (Diagenode) for 10 cycles (15 seconds on, 30 seconds off) at 4°C with the power set to high, and centrifuged at 1200g for 2 minutes. The total protein concentration in cell lysates was quantified using the BCA protein assay kit (Pierce). Protein samples (30 µg) were separated in a 4-20% Mini-PROTEAN TGX gel (BioRad) in the presence of SDS and transferred to Hybond-ECL nitrocellulose membrane (Amersham) using a Trans-Blot SD semi-dry transfer cell (BioRad). Horseradish peroxidase-conjugated mouse anti-DDDDK tag (anti-Flag M2) monoclonal antibody (1:400 dilution; Abcam, Cambridge, UK) was used for the detection of Flag-tagged ABCA2 and its variants. Rabbit anti-β-tubulin polyclonal antibody (1:2500 dilution; Abcam #ab6046) with the horseradish peroxidase-conjugated goat anti-rabbit IgG secondary antibody (1:5000 dilution; Cell Signaling Technology #7074, Danvers, MA, USA) was used for the detection of β-tubulin as a loading control. Blots were treated with Immobilon chemiluminescent reagent (EMD Millipore, Burlington, MA, USA), and proteins were visualized using a ChemiDoc XRS+ detection system (BioRad).

Cell viability measurement

HEK293 cells were seeded at a density of 8×10^4 cells per well onto poly-L-lysine-coated 48-well plates. After overnight growth, Lipofectamine 3000 Transfection Reagent was used to cotransfect the cells with 0.5 µg of expression plasmid for ABCA2, its variants, or the control plasmid, and with 0.05 µg of pEYFP. By visual inspection of EYFP fluorescence, the transfection efficiency was equally high, at least 80%, for ABCA2 WT and ABCA2 variants assayed. Transfected cells were cultured for 18 h in Opti-MEM supplemented with 3% FBS, after which the incubation continued in the regular medium, and the cells were either mock-treated or treated with medium containing 20 nM docetaxel (Cayman Chemical) and/or 0.5 µM CA-074Me (Selleck Biotechnology GmbH, Germany) for 48 h. The experiments were

repeated at least nine times in triplicate or quadruplicate wells. Cell viability was measured using the Alamar Blue (resazurin; Acros Organics) metabolic assay, as described previously[39], with slight modifications. After treatment, cells were incubated with 10% resazurin dye in DMEM for 3 hours at 37°C. Viable cells convert resazurin (blue, non-fluorescent) to resorufin (pink, highly fluorescent), which results in a change in the color and fluorescence of the incubation medium. The incubation medium of each sample was transferred in duplicate to the black 96-well plate, and resazurin reduction was measured by fluorescence (Ex/Em 540/595 nm). The background fluorescence of the resazurin solution without cells was subtracted from all samples, and the percentage of cell viability was calculated relative to the results obtained for cells transfected with the control vector.

Results

Clinical and molecular review of all cases

We reviewed the clinical and molecular data from 25 cases, including eight previously reported in the literature.[10–13] Among the 17 new individuals from 15 families, seven had heterozygous missense or in-frame variants (five were de novo and two were inherited); seven had homozygous missense or in-frame variants, and three had compound heterozygous missense or synonymous variants. According to ACMG criteria, most variants (12/17, 71%) were of uncertain significance, one was likely pathogenic, and four remained benign or likely benign even after manual curation. All individuals in the literature had either homozygous or compound heterozygous loss-of-function variants. The most prevalent symptoms were developmental delay (14/17 (82.4%) in our cohort and 7/8 (87.5%) in the literature), intellectual disability (13/17 (76.5%), 7/8 (87.5%) in literature), and seizures (9/17 (52.9%), 4/8 (50%) in literature). Abnormalities on brain MRI were more common in our cohort than in the literature (8/14, 57.1% vs 1/4, 25%); however, the individual pathologies were diverse with no consistent pattern. No evidence of myelination disorders was identified in any of the individuals. The clinical and molecular data are described in detail in Tables S1 and S2. Facial photos were obtained from individuals 1, 2, 3, 6, 7, 11, and 12. The photo from individual 3 has been uploaded to the GestaltMatcher

database[40–42] and the molecular variant has been submitted to ClinVar (Accession: VCV003362789.1). Based on the molecular data and the availability of additional materials, we decided to focus on five individuals from four families in our study cohort (individuals 1, 3, 5-7), who were also included in the cell viability assay.

In general, the frequency of symptoms in those five individuals is similar to that reported in previously published cases; however, the cohort is too small for statistical comparisons. The clinical and molecular data are described in detail in Tables S1, S2, and Supplemental File. Table 1 provides a summary, similarly to how they were presented by Inoue et al. for loss-of-function biallelic variants.[13] We did not collect data specifically about muscle hypotonia or dysarthria, so these features could not be compared. Brain magnetic resonance imaging (MRI) was performed on 2/5 (40%) individuals, and in one individual, multiple gliosis was observed (Table 1, Figure S1). Myelination disorder has not been noted in any of the individuals.

ABCA2 protein model

Using the composed ABCA2 model, assumptions can be made about the impact of single-nucleotide variants. Here, we describe all variants from the initial data collection that could be visualized in the model (Figure 1A, Supplemental Video 1). Variants included in the final cohort and functional experiments are underlined and in bold.

The variants p.Asn14Lys (individual 12), p.**Phe754Ser** (individual 5), p.**Ile786del** (individuals 6 and 7), p.**Arg926Trp** (individual 3), p.Phe1949Leu (individual 8), and p.Gly1992Arg (individual 11) are located in the transmembrane region. Changes in the physicochemical properties of mutated amino acids and their local environments can significantly affect the protein's local structure and function.

More specifically, Asn14 is involved in the stabilization of the TM domain helices, and its replacement with a larger and positively charged lysine residue is likely to cause distortions of the nearby structure and modify the geometry of the TM domain. **Phe754** (Figure 1B) is oriented towards the lipid bilayer. It partly stabilizes the angle of the alpha helix by parallel stagered π-π stacking interaction with Phe758.

Substitution to polar and non-aromatic serine probably modifies this angle and distorts the local TM domain structure. **Ile786** (Figure 1C) is oriented towards the core of the transmembrane helices. It is spatially close to Leu772, Val777, and Leu778. The deletion is likely to cause distortions in the helix it resides in, affecting the structure of the transmembrane core. **Arg926** (Figure 1D) localizes to the cytoplasmic side of the transmembrane segment enriched in positively charged amino acids. The change to a very hydrophobic amino acid, such as tryptophan, is likely to generate distortions in the environment. Phe1949 localizes in the transmembrane segment, oriented towards the lipid bilayer. It is almost symmetrical to the previously described Phe754 (Figure 1B). Phe1949 generates a T-shaped π-π stacking with Phe1946, stabilizing the local structure. Change to non-aromatic leucine cancels the π-π stacking, probably causing changes in the local structure. Gly1992 is oriented towards the core of the transmembrane helices. It is spatially proximal to Phe1949. The exchange of glycine for a large, charged amino acid, such as arginine, is likely to distort the structure of the hydrophobic core that stabilizes the transmembrane helices. Variant p.Val759Met (individual 9) is also located in the TM domain segment, oriented towards the lipid bilayer. It is a semiconservative variation, as the change in amino acid size and polarity is minor. Yet, this does not rule out a possible impact on the local protein structure.

The variants p.Arg164His (individual 14), p.Ser203_Gln204delinsGlu (individual 13), p.Gly438Val (individual 2), and p.**Asp615Glu** (individual 1) are located in the luminal domain, and variants p.Ala1284Thr (individual 10) and p.Arg2146Gly (individual 14) are in the cytoplasmic domain. Arg164 is in a solvent-oriented position, and its substitution by histidine appears to be very conservative. Although the loop in which the amino acids Ser203 and Gln204 are included could not be accurately modeled, the insertion of a negatively charged glutamine at this position is likely to affect the surface charge and, thus, the possible intermolecular contacts. Gly438 is solvent-oriented, and the change to a slightly larger and hydrophobic valine can be considered as semiconservative. Still, the distortions of the alpha helix where it is contained are possible. **Asp615** (Figure 1E) change to glutamic acid is conservative, as it involves only small size changes. Minor distortions in the local structure are possible.

Ala1284 is also oriented towards the solvent. In this environment, the change with more polar threonine is not very drastic. Hypothetically, this variant could be more significant if the particular segment is involved in protein-protein interactions. Arg2146 is located in an alpha helix, close to the position of Asp2181, in a proximal loop. The interaction between the two amino acids with opposite charges stabilizes the domain. The replacement of Arg2146 with glycine would have a destabilizing effect on this local structure.

Variants p.Ser1369Leu (individual 10) and p.Arg2394Gln (individual 4) are localized to segments that could not be included in the model. However, the variant effect prediction model AlphaMissense score[23] indicates a likely benign effect for both, and the MetaDome genetic landscape estimates both positions to be neutral to missense variation (Table S2).

In total, eight (p.Arg926Trp, p.Phe754Ser, p.Ile786del, p.Phe1949Leu, p.Gly1992Arg, p.Asn14Lys, p.Ser203_Gln204delinsGlu, p.Arg2146Gly) out of the thirteen studied variants are considered likely to have an impact on the function of the protein (Table S2).

The locations of the 14 missense variants observed in our cohort were also analyzed using the MetaDome web application, which combines data from multiple databases, including gnomAD, ClinVar, GENCODE, and Swiss-Prot, and helps predict the genetic tolerance for missense variation in specific regions (Figure 1F, Table S2). 11/14 missense variants were also in the protein model. Predictions derived from MetaDome (slightly intolerant/intolerant/highly intolerant/neutral/slightly tolerant/tolerant/highly tolerant) generally showed good concordance with the protein modeling results (likely significant, semiconservative, or conservative). All six variants classified as “likely significant” by protein modeling were predicted to be either “intolerant” or “slightly intolerant” by MetaDome. However, both variants categorized as “semiconservative” were classified as “intolerant” by MetaDome. Among the three variants considered “conservative” on the protein model, two were predicted to be “slightly intolerant,” whereas one was classified as “neutral” by MetaDome.

Metabolomics

For two male individuals (individuals 3 and 5), untargeted plasma metabolomics analysis was performed. The two samples from individual 3 were collected at ages seven and ten years, respectively, and the sample from individual 5 at eight years. The analysis of these samples revealed 492 biochemicals that could be scored against the reference population. Z-scores revealed multiple biochemicals present at levels below the 2.5th and 5th percentiles and above the 95th and 97.5th percentiles (Table S4).

Both individuals 3 and 5 harbored a heterozygous missense variant in the protein's transmembrane region. At the time of the first plasma sample, individual 3 was not taking dietary supplements and had no restrictions or medications. However, at the time of the second plasma analysis, he was taking daily oral vitamin D 400IU/d and nightly melatonin to treat sleep disorders. Individual 5 had epilepsy and thus regularly used brivaracetam to control his epileptic seizures. The time of sampling unfortunately coincided with the year when withdrawing treatment was tried, and the exact dates of starting, stopping, and restarting treatment are unknown. No other dietary supplements/restrictions or medications were reported in either of the analyzed individuals.

Analysis by metabolite groups is visualized for several more consistent groups in Figure 2. Although no metabolite groups reached statistical significance across all three samples, polyunsaturated acyl carnitines (n=3) showed a trend towards lower values (Z-scores ≤-1.14), and androgenic steroids (n=9) towards elevated values (mean Z-score ≥0.88), both are visualized in Figure S2.

Low levels (Z-score ≤ 1.6) of several sphingomyelins were observed in individual 3 (sample 1) and individual 5 (Figure S2). Analyzing metabolites separately revealed significantly lower values of β-Hydroxy β-methylglutaryl-CoA (HMG-CoA) in both samples taken from individual 3 (Z-score -2.64 and -2.6) and relatively low in the sample from individual 5 (Z-score -1). HMG-CoA is an intermediate in the mevalonate and ketogenesis pathways. Though no association between ABCA2 and cholesterol biosynthesis exists in the literature, the HMG-CoA leads to cholesterol production through the mevalonate pathway (Figure 3). Still, cholesterol was within the normal reference range for both

individuals. Since 7alpha-hydroxy-3-oxo-4-cholestenoate (7-HOCA) showed a trend towards elevation (Z-score +0.4 - +3.50) in all the samples, these changes in sterol may be due to impaired sterol and cholesterol transport and/or sequestration.

Among phospholipid degradation products, glycerophosphorylcholine and glycerophosphoethanolamine were significantly lower in both individuals (Z-score ≤-2.13 and ≤-1.04, respectively).

Several amino acids and amino acid derivatives were elevated in individual 11, who has epilepsy. This phenomenon has been described before and associated with the occurrence of epilepsy.[43]

The results of the untargeted metabolomics analysis are shown in detail in Table S4.

Experimental evaluation of ABCA2 disease-associated variants in a docetaxel toxicity cell culture model system

To shed light on the functional properties of *ABCA2* genetic variants linked to the neurodevelopmental phenotypes, we used plasmids which express either the wild type ABCA2 protein, its variant p.Asp615Glu (c.1845C>A) containing the amino acid replacement in luminal (intralysosomal) region, variants p.Phe754Ser (c.2261T>C) or p.Ile786del (c.2356_2358del) containing the change in amino acid sequence within the membrane-spanning segment or p.Arg926Trp (c.2776C>T) carrying a missense variant located within the cytoplasmic side of transmembrane domain (Figures 1A, 4A).[44] Based on MetaDome analysis, these variants are located in regions of low tolerance to variation and are classified as likely pathogenic by AlphaMissense predictions (Fig. 1F; Table S2), suggesting that these variations may disrupt protein function. To facilitate the detection of the plasmid-encoded proteins in cell culture experiments, a Flag-tag was fused to the C-terminus of the proteins. The ABCA2 expression plasmids were transfected into HEK293 cells, and the cellular lysates were analyzed by RT-qPCR and immunoblotting with an anti-Flag antibody. RT-qPCR analysis using primers which amplify a segment of the coding region of wild type ABCA2 mRNA and its variants demonstrated that the mRNA levels were similar in the cells transfected with the ABCA2 expression plasmids, indicating equal transfection

efficiency across different constructs (Figure 4B). Compared with the level of endogenous ABCA2 mRNA in the control vector-transfected cells, the cells transfected with the ABCA2 expression plasmids showed a large (an average 3000-fold) increase in ABCA2 transcript levels. In agreement with the calculated molecular weight 274 kDa of the proteins encoded by the ABCA2 plasmids, bands that migrate slightly slower than the 245 kDa marker were visible in the cells transfected with plasmids encoding wild type ABCA2 or its variants p.Asp615Glu, p.Phe754Ser, p.Ile786del, and p.Arg926Trp (Figure 4C). The presence of multiple bands appearing at a higher molecular weight than the expected size of ABCA2 may indicate posttranslational modifications, such as glycosylation[45], or unspecific protein aggregation in highly concentrated lysates of extremely hydrophobic denatured ABCA2 proteins. At the same time, in the cells transfected with the control plasmid, no band recognized by the anti-Flag antibody was observed.

While the physiological substrate of ABCA2 is still unknown, the presence of a lipocalin signature motif downstream of the ABC1 domain in ABCA2 suggests a role in binding and transporting small hydrophobic molecules, including sterols, lipids, and other related molecules.[44,46] ABCA2 has been reported to sequester lipophilic chemotherapeutic drugs into lysosomes, modulating cell survival.[44,46,47] The chemotherapy drug docetaxel is a highly lipophilic small molecule that downregulates *ABCA2* expression in HEK293 cells (Figure 4D), suggesting that ABCA2 level may play a role in the cellular response to docetaxel toxicity. Since ABCA2 is a full transporter that acts as a monomeric unit to transport substrates into lysosomes[9], we assessed the functionality of the ABCA2 variants by comparing their effects on cell sensitivity to docetaxel. Exposure of cells to docetaxel or its related compound, paclitaxel, has been shown to increase lysosomal membrane permeability and induce lysosome-mediated cell death.[48–50] We transfected HEK293 cells with the plasmids expressing ABCA2 or its variants and treated the cells with docetaxel for 48 h or left untreated. In regular growth conditions, the viability of cells transfected with the wild type ABCA2 plasmid was similar to that of cells transfected with ABCA2 variants or the control plasmid (Figure 4E). Compared to untreated cells, docetaxel exposure resulted in an average 28% reduction in viability in cells transfected with the

control plasmid, but a significantly larger reduction, 37%, was observed in cells transfected with the plasmid expressing ABCA2 (Figure 4E). In contrast to ABCA2, enforced expression of variants p.Asp615Glu, p.Phe754Ser, p.Ile786del, or p.Arg926Trp did not decrease the viability of docetaxel-exposed cells compared to cells transfected with the control plasmid. The cysteine protease cathepsin B is a major cell death-inducing enzyme that is released from lysosomes into the cytosol when the permeability of lysosomal membranes is increased.[48,49,51] To find out whether cathepsin B plays a role in the mechanism of docetaxel-induced death of cells overexpressing ABCA2, the cells were treated with CA-074 methyl ester (CA-074Me), a potent and selective cell permeable inhibitor of cathepsin B.[52] As depicted in Figure 4E, CA-074Me significantly reduced the toxic effect of docetaxel in cells transfected with the wild type ABCA2 expressing plasmid, but had no influence on cells transfected with the control plasmid. Importantly, in the presence of CA-074Me, the survival of cells transfected with the ABCA2 plasmid is similar to that of the control vector-transfected cells, indicating that the increased sensitivity of ABCA2-expressing cells to docetaxel is caused by the release of cathepsin B from lysosomes to the cytosol. In conclusion, the data suggest that ABCA2-dependent increased cytotoxicity might result from the ABCA2-mediated lysosomal accumulation of docetaxel. Unlike ABCA2, its variants p.Asp615Glu, p.Phe754Ser, p.Ile786del, and p.Arg926Trp do not potentiate cell death in docetaxel-exposed cells, possibly reflecting a lost or strongly reduced ability of the disease-associated variants to function as a transporter.

Discussion

This study collected data on 17 individuals with mono- or biallelic variants in the *ABCA2* gene, and five individuals were selected for further study: three with heterozygous *de novo* missense variants and two with homozygous in-frame deletions in *ABCA2*. All five had developmental delay and intellectual disability, in addition to other, more variable symptoms, similar to the autosomal recessive phenotype described previously in eight patients.[10–13] The additional symptoms included seizures, ataxia, limb incoordination, and microcephaly (Table 1, Table S1).

The protein model predicts the least impact for the Asp615 change to glutamic acid (Individual 1) and indeed, this individual has one of the mildest phenotypes. Despite variable *in silico* predictions ranging from benign supporting to likely pathogenic, this variant could still affect protein function. A similar conservative change of Asp->Glu in the GAA gene (HGNC:4065, MIM: 606800) has been shown to be pathogenic in a patient with late-onset Pompe disease (MIM: 621314).[53] The three variants (p.Arg926Trp, p.Ile786del, p.Phe754Ser) located in the transmembrane region have a stronger computational support for being pathogenic.

The cell viability assays with the four variants (p.Asp615Glu, p.Phe754Ser, p.Ile786del, and p.Arg926Trp) indicated a lost or strongly reduced ability to function as a transporter. These changes in the amino acid sequence of the ABCA2 variants are located in and around the first transmembrane domain, and amino acid substitutions in this region are expected to affect the transport of substrates.[54] The function of ABCA2 variants depends not only on their ability to transport substrates across the membrane, but also on their correct subcellular localization. Schmitz and Kaminski[55] have reported that a cluster of lysosomal targeting motifs is identifiable at the ABCA2 C-terminal region, and Beers et al.[56] have demonstrated that a highly conserved targeting motif xLxxKN located within the N-terminus of ABCA transporters (including ABCA2) directs the proteins to early post-Golgi compartments. Also, two di-leucine (or isoleucine) motifs, which represent the second class of lysosomal and endosomal targeting signals, are localized close to the ABCA2 C-terminus.[55,57] The changes in the amino acid sequence of ABCA2 variants characterized in the cell viability assays are located far from the ABCA2 targeting motifs mentioned above. Thus, based on the current knowledge, it seems likely that the amino acid variations analyzed in this study do not affect ABCA2 targeting to lysosomes.

Although we observed altered function compared with wild type, there were no significant differences between the variants themselves, despite their different computational predictions and different zygosity in patients. It was an unexpected result, but it might be explained by a more complex pathomechanism *in vivo* than what we were able to study in our experiment. Autosomal recessive inheritance typically indicates variants with a loss-of-function mechanism; however, autosomal

dominant inheritance can result from loss-of-function, gain-of-function, or dominant-negative effects.[14] The genotype-phenotype relationships can be very complex and require large cohorts to understand, as demonstrated in phosphomannomutase 2 deficiency (MIM: 212065), for example.[58] The precise pathomechanism of different variants and combinations needs further elucidation; however, our sample size and resources were limited. Still, the altered function of the variant ABCA2 suggests a biological effect *in vivo* as well.

ABCA2 is predominantly expressed in brain tissue; neurological defects observed in Abca2 knockout mice are consistent with aberrant myelination.[9] In our cohort, brain MRI was done in only two individuals – one was normal, and the second had gliosis (Figure S1). However, myelination defects have not been described in previously reported individuals either.

Analysis of brain lipids of Abca2 knockout mice aged 4 to 64 weeks showed consistently decreased sphingomyelin levels, although no significant changes in cholesterol or glycerophospholipid levels were observed. Lipid analysis of myelin fractions revealed a similar decrease in sphingomyelin levels and a two-fold increase in ganglioside GM1 compared to wild type littermates. These results indicate that ABCA2 modulates intracellular sphingolipid metabolism in the brain.[8,9] Considering the difficulties in obtaining brain tissue for research, we decided to find possible metabolic abnormalities in blood plasma instead. We performed an exploratory untargeted metabolomics analysis of three plasma samples obtained from two affected individuals. Our results did not reveal a consistent downregulation of sphingomyelins, possibly due to differences in tissue types or confounding factors in patient samples not present in animal models. Interestingly, we observed a downward trend in polyunsaturated acylcarnitines. The lack of statistical significance may be due to the small number of metabolites in this group. Plasma metabolomics is a promising field of research, and a larger cohort would allow for drawing more definitive conclusions.

Strengths and limitations

The current study had several limitations, notably the small sample size and limited functional tests. The strengths are protein modeling, cell viability assays, and thorough clinical descriptions, which aid us in understanding the diverse phenotypic spectrum of *ABCA2* variants. The complex and heterogeneous phenotypes warrant further investigation in larger cohorts and through additional functional studies. Future metabolic studies could include additional plasma samples from other affected individuals, analysis of multiple samples from the same individuals, and testing of additional sample types, such as urine and cerebrospinal fluid.

Conclusions

The present study describes individuals with mono- and biallelic variants in the *ABCA2* gene that are the best candidates to explain their neurodevelopmental disorder. Cell viability assays with four variants revealed an altered ABCA2 pump function compared to wild type. However, further functional studies are needed to understand the exact pathomechanism.

Supplemental information

The supplemental materials include four tables, a supplemental note with case reports, and supplemental figures (Figure S1 and S2), and a video. Table S1 provides a clinical overview of the cohort; Table S2 lists *ABCA2* molecular variants with pathogenicity scores; Table S3 details the sequencing platforms and analysis pipelines; and Table S4 presents results from the untargeted metabolomics analysis. Supplemental Note with case reports contains updated clinical descriptions of eleven individuals. Figure S1 contains the MRI images of individual 5, and Figure S2 shows three subplots of the untargeted metabolomics data; Supplemental Video 1 features an animated 3D model of the ABCA2 protein.

Acknowledgements

The authors are grateful to the study participants and their families. The authors also thank the European Reference Network for Rare Malformation Syndromes and Rare Intellectual and Neurodevelopmental Disorders (ERN-ITHACA) for fruitful collaboration.

This work is supported by Estonian Research Council grants PUT355, PRG471, PRG2040, PRG1475 and PSG774; The Broad Institute Center for Mendelian Genomics (UM1HG008900) is funded by the National Human Genome Research Institute (NHGRI) with supplemental funding provided by the National Heart, Lung, and Blood Institute and the National Eye Institute (sequencing and analysis), and NHGRI grants U01HG011755 and R01HG009141 (analysis). M.H.W. is supported by K23HD102589. This work was also supported by Spanish government grants RTI2018-094434-B-I00, PID2021-126625OB-I00 (MCIN/AEI/10.13039/501100011033/FEDER,EU.2022) and DTS20-00024 (ISCIII) to P.G-P., as well as funds from the European JPIAMR network "EPIC-Alliance" to P.G-P. The computational support of the "Centro de Computación Científica CCC-UAM" is gratefully recognized. A.R. and A.M.P. received funding from GENERA FSC 2014-2020 - Genoma mEdiciNa pERsonalizzatA, - POS-Ministero della Salute T3-AN-04 to A.R.; EU H2020-SC1-FA-DTS-2018–2020, International consortium for integrative genomics prediction - Grant Agreement No. 101016775 to A.R.; ERDERA Diagnostic Research Workstream to A.R.

Author contributions

Conceptualization: Karit Reinson, Katrin Õunap, and Tõnis Örd.

Resources: Kaisa T. Oja, Karit Reinson, Christiane Zweier, Georgia Vasileiou, Issam A. Alkhawaja, Thomas Wirth, Steffen Syrbe, Konrad Platzer, Suad Alyamani, Fowzan S. Alkuraya, Marie Vidailhet, Ke Su, Shaohua Fan, Yu Ma, Yi Wang, Alessandra Renieri, Anna Maria Pinto, Farah Almadhoun, Kari Magnussen, Andrea K. Petersen, Olaf Bodamer, Talal Alanzi, Sarar Mohammed, Hadeel Alrabee, Bader Alhaddad, Khadijah Bakur, and Amber Begtrup.

Data curation: Kaisa T. Oja, Karit Reinson, Mihkel Ilisson, and Sander Pajusalu.

Investigation: Kaisa T. Oja, Karit Reinson, Daima Örd, Bryan M. Wittmann, Adam D. Kennedy, Karen DeBalsi, David Ros-Pardo, Iñigo Marcos-Alcalde, Paulino Gómez-Puertas, Nicole Fleischer, and Tõnis Örd.

Visualization: Daima Örd, Karen DeBalsi, David Ros-Pardo, Iñigo Marcos-Alcalde, and Paulino Gómez-Puertas.

Writing – original draft: Kaisa T. Oja, Karit Reinson, Adam D. Kennedy, David Ros-Pardo, and Daima Örd.

Supervision: Sander Pajusalu and Katrin Õunap.

Writing – review & editing: All authors.

Declaration of interests

Authors B.M.W, A.K., and K.D. were employed by company Metabolon. K. B. and B.A were employed by Lifera Omics.

The remaining authors declare that the research was conducted in the absence of any commercial or financial relationships that could be construed as a potential conflict of interest.

Declaration of generative AI and AI-assisted technologies in the writing process

During the preparation of this work the authors used Grammarly and chatGPT in order to improve readability and correct grammar. After using these tools, the authors reviewed and edited the content as needed and take full responsibility for the content of the publication.

Data and Code Availability

The published article includes all datasets generated or analyzed during this study.

Web Resources

Alphafold-3, https://alphafoldserver.com/

Clinvar, https://www.ncbi.nlm.nih.gov/clinvar/

GENCODE, https://www.gencodegenes.org/

GeneMatcher, https://genematcher.org/

GestaltMatcher, https://www.gestaltmatcher.org/

GnomAD, https://gnomad.broadinstitute.org/

Metadome, https://www.metadome.app/metadome/

MolProbity, http://molprobity.biochem.duke.edu/

ModFOLD9, https://www.reading.ac.uk/bioinf/ModFOLD/

OMIM, http://www.omim.org/

Pymol Molecular Graphics System, https://pymol.org/

RefSeq, https://www.ncbi.nlm.nih.gov/refseq/

SWISS-MODEL server, http://swissmodel.expasy.org

UniProt, https://www.uniprot.org/

Variant Validator, https://www.variantvalidator.org/

Varsome, https://varsome.com/

References

1. Vasiliou, V., Vasiliou, K., and Nebert, D.W. (2009). Human ATP-binding cassette (ABC) transporter family. Hum. Genomics *3*, 281–290. https://doi.org/10.1186/1479-7364-3-3-281.

2. ter Beek, J., Guskov, A., and Slotboom, D.J. (2014). Structural diversity of ABC transporters. J. Gen. Physiol. *143*, 419–435. https://doi.org/10.1085/jgp.201411164.

3. Juliano, R.L., and Ling, V. (1976). A surface glycoprotein modulating drug permeability in Chinese hamster ovary cell mutants. Biochim. Biophys. Acta *455*, 152–162. https://doi.org/10.1016/0005-2736(76)90160-7.

4. Wang, J.-Q., Wu, Z.-X., Yang, Y., Teng, Q.-X., Li, Y.-D., Lei, Z.-N., Jani, K.A., Kaushal, N., and Chen, Z.-S. (2021). ATP-binding cassette (ABC) transporters in cancer: A review of recent updates. J. Evid.-Based Med. *14*, 232–256. https://doi.org/10.1111/jebm.12434.

5. Luciani, M.F., Denizot, F., Savary, S., Mattei, M.G., and Chimini, G. (1994). Cloning of two novel ABC transporters mapping on human chromosome 9. Genomics *21*, 150–159. https://doi.org/10.1006/geno.1994.1237.

6. Davis, W. (2014). The ATP-binding cassette transporter-2 (ABCA2) regulates esterification of plasma membrane cholesterol by modulation of sphingolipid metabolism. Biochim. Biophys. Acta *1841*, 168–179. https://doi.org/10.1016/j.bbalip.2013.10.019.

7. Davis, W. (2015). The ATP-Binding Cassette Transporter-2 (ABCA2) Overexpression Modulates Sphingosine Levels and Transcription of the Amyloid Precursor Protein (APP) Gene. Curr. Alzheimer Res. *12*, 847–859. https://doi.org/10.2174/1567205012091510191058 34.

8. Sakai, H., Tanaka, Y., Tanaka, M., Ban, N., Yamada, K., Matsumura, Y., Watanabe, D., Sasaki, M., Kita, T., and Inagaki, N. (2007). ABCA2 deficiency results in abnormal sphingolipid metabolism in mouse brain. J. Biol. Chem. *282*, 19692–19699. https://doi.org/10.1074/jbc.M611056200.

9. Davis, W., and Tew, K.D. (2018). ATP-binding cassette transporter-2 (ABCA2) as a therapeutic target. Biochem. Pharmacol. *151*, 188–200. https://doi.org/10.1016/j.bcp.2017.11.018.

10. Maddirevula, S., Alzahrani, F., Al-Owain, M., Al Muhaizea, M.A., Kayyali, H.R., AlHashem, A., Rahbeeni, Z., Al-Otaibi, M., Alzaidan, H.I., Balobaid, A., et al. (2019). Autozygome and high throughput confirmation of disease genes candidacy. Genet. Med. Off. J. Am. Coll. Med. Genet. *21*, 736–742. https://doi.org/10.1038/s41436-018-0138-x.

11. Aslam, F., and Naz, S. (2019). Ataxia and dysarthria due to an ABCA2 variant: Extension of the phenotypic spectrum. Parkinsonism Relat. Disord. *64*, 328–331. https://doi.org/10.1016/j.parkreldis.2019.04.017.

12. Hu, H., Kahrizi, K., Musante, L., Fattahi, Z., Herwig, R., Hosseini, M., Oppitz, C., Abedini, S.S., Suckow, V., Larti, F., et al. (2019). Genetics of intellectual disability in consanguineous families. Mol. Psychiatry *24*, 1027–1039. https://doi.org/10.1038/s41380-017-0012-2.

13. Inoue, Y., Tsuchida, N., Kim, C.A., de Oliveira Stephan, B., Castro, M.A.A., Honjo, R.S., Bertola, D.R., Uchiyama, Y., Hamanaka, K., Fujita, A., et al. (2024). Novel compound heterozygous ABCA2 variants cause IDPOGSA, a variable phenotypic syndrome with intellectual disability. J. Hum. Genet. *69*, 163–167. https://doi.org/10.1038/s10038-024-01219-8.

14. Ezer, S., Sido, T., Rips, J., Hoffman Lipschuetz, R., Fuchs, A., Abu-Libdeh, B., Chervinsky, E., Damseh, N.S., Danial-Farran, N., Morani, I., et al. (2025). Exploring the unique characteristics of genes with dual autosomal dominant and recessive inheritance: mechanisms, phenotypes and candidate identification. J. Med. Genet. *62*, 682–692. https://doi.org/10.1136/jmg-2025-110872.

15. Brooks-Wilson, A., Marcil, M., Clee, S.M., Zhang, L.-H., Roomp, K., van Dam, M., Yu, L., Brewer, C., Collins, J.A., Molhuizen, H.O.F., et al. (1999). Mutations in ABC1 in Tangier disease and familial high-density lipoprotein deficiency. Nat. Genet. *22*, 336–345. https://doi.org/10.1038/11905.

16. Efthymiou, S., Scala, M., Nagaraj, V., Ochenkowska, K., Komdeur, F.L., Liang, R.A., Abdel-Hamid, M.S., Sultan, T., Barøy, T., Van Ghelue, M., et al. (2024). Novel loss-of-function variants expand ABCC9-related intellectual disability and myopathy syndrome. Brain *147*, 1822–1836. https://doi.org/10.1093/brain/awae010.

17. Smeland, M.F., McClenaghan, C., Roessler, H.I., Savelberg, S., Hansen, G.Å.M., Hjellnes, H., Arntzen, K.A., Müller, K.I., Dybesland, A.R., Harter, T., et al. (2019). ABCC9-related Intellectual disability Myopathy Syndrome is a KATP channelopathy with loss-of-function mutations in ABCC9. Nat. Commun. *10*, 4457. https://doi.org/10.1038/s41467-019-12428-7.

18. Pais, L.S., Snow, H., Weisburd, B., Zhang, S., Baxter, S.M., DiTroia, S., O'Heir, E., England, E., Chao, K.R., Lemire, G., et al. (2022). seqr: A web-based analysis and collaboration tool for rare disease genomics. Hum. Mutat. *43*, 698–707. https://doi.org/10.1002/humu.24366.

19. Sobreira, N., Schiettecatte, F., Valle, D., and Hamosh, A. (2015). GeneMatcher: a matching tool for connecting investigators with an interest in the same gene. Hum. Mutat. *36*, 928–930. https://doi.org/10.1002/humu.22844.

20. Philippakis, A.A., Azzariti, D.R., Beltran, S., Brookes, A.J., Brownstein, C.A., Brudno, M., Brunner, H.G., Buske, O.J., Carey, K., Doll, C., et al. (2015). The Matchmaker Exchange: a platform for rare disease gene discovery. Hum. Mutat. *36*, 915–921. https://doi.org/10.1002/humu.22858.

21. Schubach, M., Maass, T., Nazaretyan, L., Röner, S., and Kircher, M. (2024). CADD v1.7: using protein language models, regulatory CNNs and other nucleotide-level scores to improve genome-wide variant predictions. Nucleic Acids Res. *52*, D1143–D1154. https://doi.org/10.1093/nar/gkad989.

22. Ioannidis, N.M., Rothstein, J.H., Pejaver, V., Middha, S., McDonnell, S.K., Baheti, S., Musolf, A., Li, Q., Holzinger, E., Karyadi, D., et al. (2016). REVEL: An Ensemble Method for Predicting the Pathogenicity of Rare Missense Variants. Am. J. Hum. Genet. *99*, 877–885. https://doi.org/10.1016/j.ajhg.2016.08.016.

23. Cheng, J., Novati, G., Pan, J., Bycroft, C., Žemgulytė, A., Applebaum, T., Pritzel, A., Wong, L.H., Zielinski, M., Sargeant, T., et al. (2023). Accurate proteome-wide missense variant effect prediction with AlphaMissense. Science *381*, eadg7492. https://doi.org/10.1126/science.adg7492.

24. Li, C., Zhi, D., Wang, K., and Liu, X. (2022). MetaRNN: differentiating rare pathogenic and rare benign missense SNVs and InDels using deep learning. Genome Med. *14*, 115. https://doi.org/10.1186/s13073-022-01120-z.

25. Wiel, L., Baakman, C., Gilissen, D., Veltman, J.A., Vriend, G., and Gilissen, C. (2019). MetaDome: Pathogenicity analysis of genetic variants through aggregation of homologous human protein domains. Hum. Mutat. *40*, 1030–1038. https://doi.org/10.1002/humu.23798.

26. Richards, S., Aziz, N., Bale, S., Bick, D., Das, S., Gastier-Foster, J., Grody, W.W., Hegde, M., Lyon, E., Spector, E., et al. (2015). Standards and Guidelines for the Interpretation of Sequence Variants: A Joint Consensus Recommendation of the American College of Medical Genetics and Genomics and the Association for Molecular Pathology. Genet. Med. Off. J. Am. Coll. Med. Genet. *17*, 405–424. https://doi.org/10.1038/gim.2015.30.

27. Kopanos, C., Tsiolkas, V., Kouris, A., Chapple, C.E., Albarca Aguilera, M., Meyer, R., and Massouras, A. (2019). VarSome: the human genomic variant search engine. Bioinformatics *35*, 1978–1980. https://doi.org/10.1093/bioinformatics/bty897.

28. Freeman, P.J., Hart, R.K., Gretton, L.J., Brookes, A.J., and Dalgleish, R. (2018). VariantValidator: Accurate validation, mapping, and formatting of sequence variation descriptions. Hum. Mutat. *39*, 61–68. https://doi.org/10.1002/humu.23348.

29. Qian, H., Zhao, X., Cao, P., Lei, J., Yan, N., and Gong, X. (2017). Structure of the Human Lipid Exporter ABCA1. Cell *169*, 1228-1239.e10. https://doi.org/10.1016/j.cell.2017.05.020.

30. Scortecci, J.F., Molday, L.L., Curtis, S.B., Garces, F.A., Panwar, P., Van Petegem, F., and Molday, R.S. (2021). Cryo-EM structures of the ABCA4 importer reveal mechanisms underlying substrate

binding and Stargardt disease. Nat. Commun. *12*, 5902. https://doi.org/10.1038/s41467-021-26161-7.

31. Xie, T., Zhang, Z., Fang, Q., Du, B., and Gong, X. (2021). Structural basis of substrate recognition and translocation by human ABCA4. Nat. Commun. *12*, 3853. https://doi.org/10.1038/s41467-021-24194-6.

32. Williams, C.J., Headd, J.J., Moriarty, N.W., Prisant, M.G., Videau, L.L., Deis, L.N., Verma, V., Keedy, D.A., Hintze, B.J., Chen, V.B., et al. (2018). MolProbity: More and better reference data for improved all-atom structure validation. Protein Sci. Publ. Protein Soc. *27*, 293–315. https://doi.org/10.1002/pro.3330.

33. Studer, G., Rempfer, C., Waterhouse, A.M., Gumienny, R., Haas, J., and Schwede, T. (2020). QMEANDisCo-distance constraints applied on model quality estimation. Bioinformatics *36*, 1765–1771. https://doi.org/10.1093/bioinformatics/btz828.

34. McGuffin, L.J., and Alharbi, S.M.A. (2024). ModFOLD9: A Web Server for Independent Estimates of 3D Protein Model Quality. J. Mol. Biol. *436*, 168531. https://doi.org/10.1016/j.jmb.2024.168531.

35. Abramson, J., Adler, J., Dunger, J., Evans, R., Green, T., Pritzel, A., Ronneberger, O., Willmore, L., Ballard, A.J., Bambrick, J., et al. (2024). Accurate structure prediction of biomolecular interactions with AlphaFold 3. Nature *630*, 493–500. https://doi.org/10.1038/s41586-024-07487-w.

36. Lichtenberg, S., Trifonova, O.P., Maslov, D.L., Balashova, E.E., and Lokhov, P.G. (2021). Metabolomic Laboratory-Developed Tests: Current Status and Perspectives. Metabolites *11*, 423. https://doi.org/10.3390/metabo11070423.

37. Ford, L., Kennedy, A.D., Goodman, K.D., Pappan, K.L., Evans, A.M., Miller, L.A.D., Wulff, J.E., Wiggs, B.R., Lennon, J.J., Elsea, S., et al. (2020). Precision of a Clinical Metabolomics Profiling Platform for Use in the Identification of Inborn Errors of Metabolism. J. Appl. Lab. Med. *5*, 342–356. https://doi.org/10.1093/jalm/jfz026.

38. Örd, T., Örd, D., Kuuse, S., Plaas, M., and Örd, T. (2012). Trib3 is regulated by IL-3 and affects bone marrow-derived mast cell survival and function. Cell. Immunol. *280*, 68–75. https://doi.org/10.1016/j.cellimm.2012.11.011.

39. Örd, T., Örd, D., Kaikkonen, M.U., and Örd, T. (2021). Pharmacological or TRIB3-Mediated Suppression of ATF4 Transcriptional Activity Promotes Hepatoma Cell Resistance to Proteasome Inhibitor Bortezomib. Cancers *13*, 2341. https://doi.org/10.3390/cancers13102341.

40. Õunap, K. (2024). A case with coarse facial features, mandibular prognathia, and macrotia, in combination with neurobehavioral abnormalities and a missense variant in ABCA2. Version Version 1 (GestaltMatcher Database). https://doi.org/10.60723/13108 https://doi.org/10.60723/13108.

41. Hsieh, T.-C., Bar-Haim, A., Moosa, S., Ehmke, N., Gripp, K.W., Pantel, J.T., Danyel, M., Mensah, M.A., Horn, D., Rosnev, S., et al. (2022). GestaltMatcher facilitates rare disease matching using facial phenotype descriptors. Nat. Genet. *54*, 349–357. https://doi.org/10.1038/s41588-021-01010-x.

42. Lesmann, H., Hustinx, A., Moosa, S., Klinkhammer, H., Marchi, E., Caro, P., Abdelrazek, I.M., Pantel, J.T., Hagen, M. ten, Thong, M.-K., et al. (2024). GestaltMatcher Database - A global reference for

facial phenotypic variability in rare human diseases. Preprint at medRxiv, https://doi.org/10.1101/2023.06.06.23290887 https://doi.org/10.1101/2023.06.06.23290887.

43. Lee, W.-T. (2011). Disorders of amino acid metabolism associated with epilepsy. Brain Dev. *33*, 745–752. https://doi.org/10.1016/j.braindev.2011.06.014.

44. Vulevic, B., Chen, Z., Boyd, J.T., Davis, W., Walsh, E.S., Belinsky, M.G., and Tew, K.D. (2001). Cloning and characterization of human adenosine 5'-triphosphate-binding cassette, sub-family A, transporter 2 (ABCA2). Cancer Res. *61*, 3339–3347.

45. Zhao, L.X., Zhou, C.J., Tanaka, A., Nakata, M., Hirabayashi, T., Amachi, T., Shioda, S., Ueda, K., and Inagaki, N. (2000). Cloning, characterization and tissue distribution of the rat ATP-binding cassette (ABC) transporter ABC2/ABCA2. Biochem. J. *350 Pt 3*, 865–872.

46. Szakacs, G., and Abele, R. (2020). An inventory of lysosomal ABC transporters. FEBS Lett. *594*, 3965–3985. https://doi.org/10.1002/1873-3468.13967.

47. Kim, M.S., Yang, S.H., and Kim, M.S. (2023). Role of ABCA2 and its single nucleotide polymorphisms (4873T>A and 4879G>C) in the regulation of multi-drug resistance in oral squamous carcinoma cells. Biochem. Biophys. Res. Commun. *666*, 1–9. https://doi.org/10.1016/j.bbrc.2023.05.021.

48. Mediavilla-Varela, M., Pacheco, F.J., Almaguel, F., Perez, J., Sahakian, E., Daniels, T.R., Leoh, L.S., Padilla, A., Wall, N.R., Lilly, M.B., et al. (2009). Docetaxel-induced prostate cancer cell death involves concomitant activation of caspase and lysosomal pathways and is attenuated by LEDGF/p75. Mol. Cancer *8*, 68. https://doi.org/10.1186/1476-4598-8-68.

49. Bröker, L.E., Huisman, C., Span, S.W., Rodriguez, J.A., Kruyt, F.A.E., and Giaccone, G. (2004). Cathepsin B mediates caspase-independent cell death induced by microtubule stabilizing agents in non-small cell lung cancer cells. Cancer Res. *64*, 27–30. https://doi.org/10.1158/0008-5472.can-03-3060.

50. Trybus, W., Trybus, E., and Król, T. (2023). Lysosomes as a Target of Anticancer Therapy. Int. J. Mol. Sci. *24*, 2176. https://doi.org/10.3390/ijms24032176.

51. Boya, P., and Kroemer, G. (2008). Lysosomal membrane permeabilization in cell death. Oncogene *27*, 6434–6451. https://doi.org/10.1038/onc.2008.310.

52. Yoon, M.C., Christy, M.P., Phan, V.V., Gerwick, W.H., Hook, G., O'Donoghue, A.J., and Hook, V. (2022). Molecular Features of CA-074 pH-Dependent Inhibition of Cathepsin B. Biochemistry *61*, 228–238. https://doi.org/10.1021/acs.biochem.1c00684.

53. Hermans, M.M., de Graaff, E., Kroos, M.A., Wisselaar, H.A., Willemsen, R., Oostra, B.A., and Reuser, A.J. (1993). The conservative substitution Asp-645-->Glu in lysosomal alpha-glucosidase affects transport and phosphorylation of the enzyme in an adult patient with glycogen-storage disease type II. Biochem. J. *289*, 687–693. https://doi.org/10.1042/bj2890687.

54. Mack, J.T., Townsend, D.M., Beljanski, V., and Tew, K.D. (2007). The ABCA2 transporter: intracellular roles in trafficking and metabolism of LDL-derived cholesterol and sterol-related compounds. Curr. Drug Metab. *8*, 47–57. https://doi.org/10.2174/138920007779315044.

55. Schmitz, G., and Kaminski, W.E. (2002). ABCA2: a candidate regulator of neural transmembrane lipid transport. Cell. Mol. Life Sci. CMLS *59*, 1285–1295. https://doi.org/10.1007/s00018-002-8508-5.

56. Beers, M.F., Hawkins, A., Shuman, H., Zhao, M., Newitt, J.L., Maguire, J.A., Ding, W., and Mulugeta, S. (2011). A novel conserved targeting motif found in ABCA transporters mediates trafficking to early post-Golgi compartments. J. Lipid Res. *52*, 1471–1482. https://doi.org/10.1194/jlr.M013284.

57. Hunziker, W., and Geuze, H.J. (1996). Intracellular trafficking of lysosomal membrane proteins. BioEssays News Rev. Mol. Cell. Dev. Biol. *18*, 379–389. https://doi.org/10.1002/bies.950180508.

58. Pajusalu, S., Vals, M.-A., Serrano, M., Witters, P., Cechova, A., Honzik, T., Edmondson, A.C., Ficicioglu, C., Barone, R., De Lonlay, P., et al. (2024). Genotype/Phenotype Relationship: Lessons From 137 Patients With PMM2-CDG. Hum. Mutat. *2024*, 8813121. https://doi.org/10.1155/2024/8813121.

Figure titles and legends

Figure 1. 3D structure model of human ATP-binding cassette sub-family A member 2 (ABCA2) and the genetic tolerance landscape of ABCA2. (A) The approximate positions of the lipid membrane, cytosol, and lumen are indicated. The probable positions of three phospholipids and two possible oligosaccharide molecules attached to the asparagine residues Asn477 and Asn1678 are included. The position in the model of the amino acids involved in the variants discussed in the text is labeled: Asn14, Arg164, Gly438, Asp615, Phe754, Val759, Ile786, Arg926, Ala1284, Phe1949, Gly1992, and Arg2146 (red spheres). The red circle indicates the approximate positions of the residues Ser203 and Gln204, which are not included in the model. Panels B, C, D, and E illustrate the locations of the amino acid variants included in the final cohort and functional experiments. **(B)** Left: Location of Phe754, maintaining a parallel staggered π-π stacking interaction with Phe758. Right: The location of Phe1949 is also shown, in a position nearly symmetrical to Phe754 and maintaining a T-shaped staggered π-π stacking interaction with Phe1946. **(C)** Location of Ile786, surrounded by the hydrophobic residues Leu772, Val777, and Leu778. **(D)** Position of Arg926, as well as several nearby positively charged residues: Lys1001, Lys1010, Arg1057, and Arg1064. **(E)** Location of Asp615 and the polar amino acids that contact it: Gln611 and Arg613. The position of Asn477 and a potentially bound oligosaccharide molecule (N-glycan-Asn477) is indicated. **(F)** The genetic tolerance landscape of ABCA2 (GENCODE: ENST00000341511.11, RefSeq: NM_001606.5, UniProt: Q9BZC7-3) in Metadome (Wiel et al, 2019). The amino acid positions of missense variants in our cohort are annotated on the protein schematic

along with their nonsynonymous to synonymous ratio (dn/ds score). The colorscale is shown in the figure, with yellow indicating neutral positions, light orange indicating slightly intolerant positions, and dark orange indicating intolerant positions. Underlining indicates the position of variants included in our cell viability assay.

Figure 2. The summarized results of untargeted metabolomics analysis from three plasma samples of two individuals. The boxplots show the main trends in different subpathways. Asterisks denote statistical significance (*p<0.05, **p<0.01) from reference cohort. P-values are FDR-corrected for multiple testing by Benjamini-Hochberg method. Abbreviations: s – sample.

Figure 3. Cholesterol production through the mevalonate pathway. The green and red arrows indicate compounds that were respectively lower or higher in the plasma samples of individuals with *ABCA2* variants compared to the reference cohorts. The black arrows indicate the metabolic reactions and the grey rectangles differntiate enzymes from metabolites.

Figure 4. The influence of ABCA2 and its disease-associated variants p.Asp615Glu, p.Phe754Ser, p.Ile786del, and p.Arg926Trp on the sensitivity of HEK293 cells to docetaxel.

(A) Schematic representation of wild type (WT) ABCA2 and its disease-associated variants (p.Asp615Glu, p.Phe754Ser, p.Ile786del, and p.Arg926Trp), which were expressed from the plasmids and studied in the cell viability assays. The ABCA2 ATP-binding cassettes (ABC1, ABC2) and hydrophobic transmembrane domains (TMD1, TMD2), each containing six membrane-spanning regions (grey rectangles), are indicated.

(B, C) Quantification of ABCA2 mRNA by RT-qPCR (**B**; *n* = 4) and detection of Flag-tagged ABCA2 protein by immunoblot (**C**) in HEK293 cells transfected with the expression plasmids encoding WT ABCA2, its variants (p.Asp615Glu, p.Phe754Ser, p.Ile786del, and p.Arg926Trp) or control vector (ctrl vector). In **B**, the expression levels of *ABCA2* were normalized to *GAPDH* and mean values ± SD are presented

relative to the expression level of endogenous *ABCA2* in cells transfected with an empty ctrl vector. In **C**, cell lysates were analyzed by anti-Flag antibody; β-tubulin was used as a loading control.

(D) Quantification of ABCA2 mRNA by RT-qPCR (n = 4) in HEK293 cells treated with 20 nM docetaxel for 24 h or left untreated. The expression levels of *ABCA2* were normalized to *GAPDH* and mean values ± SD are presented relative to the level of ABCA2 mRNA in untreated cells. ** $p < 0.005$ by two-tailed t test.

(E) Viability of HEK293 cells transfected with the expression plasmids encoding ABCA2, its variants (p.Asp615Glu, p.Phe754Ser, p.Ile786del and p.Arg926Trp) or the control vector and left untreated or treated with 20 nM docetaxel for 48 h. Where indicated, 0.5 µM CA-074Me, the inhibitor of cathepsin B, was added. Viability was determined by the Alamar Blue fluorometric assay and the mean percentage of cell viability ± SD from nine to thirteen independent experiments is presented relative to the viability of untreated cells transfected with the control vector. Dotted line denotes mean viability of cells transfected with plasmid expressing ABCA2 and exposed to docetaxel. * $p < 0.05$, ** $p < 0.005$, *** $p < 0.0005$ using two-tailed t tests followed by Holm-Bonferroni correction comparing viabilities within different treatment groups to the viability of control vector-transfected cells and ABCA2 overexpressing cells in the same treatment group. In addition, to determine the effect of CA-074Me on docetaxel-induced cell death, the viability of control vector-transfected cells exposed to docetaxel with and without CA-074Me were compared.

1 **Tables**

2 **Table 1. Summary of clinical characteristics in our cohort and cases reported in literature.[10–13] The table layout is based on the summary by Inoue et al.[13]**

	Case 1	Case 3	Case 5	Cases 6 and 7		Cohort with cell assays	Others in our cohort	Literature summary[10–13]
Cases in family/cohort	1	1	1	2		5 cases in 4 families	12 cases in 11 families	8 cases in 5 families
Sex	M	M	M	F	F	M: 3; F: 2	M : 5; F : 7	M: 4, F: 4
Age (years)	21	8	7	16	NA	7–21	1–76	5–28
Ethnicity	European	European	European	Saudi Arabian		Variable	Variable	Variable
Consanguinity	no	no	no	yes		1/4 families	4/11 families	4/5 families
Zygosity	HTZ (de novo)	HTZ (de novo)	HTZ (de novo)	HMZ (inh)		3 HTZ (de novo), 2 HMZ	2 HTZ (de novo), 2 HTZ (inh), 5 HMZ, 3 cHTZ	7 HMZ, 1 cHTZ
Nucleotide and amino acid change (NM_001606.5)	c.1845C>A p.(Asp615Glu)	c.2776C>T p.(Arg926Trp)	c.2261T>C p.(Phe754Ser)	c.2356_2358del p.(Ile786del)		Variable	Variable	Variable
Developmental delay	+	+	+	+	+	100% (5/5)	75% (9/12)	87.5% (7/8)
Intellectual disability	+ (mild)	+ (moderate)	+ (learning dif.)	+ (severe)	+ (mild)	100% (5/5)	66.7% (8/12)	87.5% (7/8)
Seizures	-	-	+	+	+	60% (3/5)	50% (6/12)	50.0% (4/8)
Ataxia	-	-	-	+	-	20% (1/5)	41.7% (5/12)	50% (4/8)
Limb incoordination	-	-	+	+	-	40% (2/5)	50% (6/12)	37.5% (3/8)
Brain pathologies (MRI)	NA	-	gliosis multiple	NA	NA	50% (1/2)	77.8% (7/9)	25.0% (1/4)
Facial dysmorphism	+	+	-	-	-	40% (2/5)	25% (3/12)	12.5% (1/8)
Microcephaly	+	-	+	-	-	40% (2/5)	33.3% (2/6)	37.5% (3/8)

Abbreviations: AR – autosomal recessive, HMZ – homozygous, HTZ – heterozygous, cHTZ – compound heterozygous, NA – not available, learning dif. – learning difficulty, inh – inherited

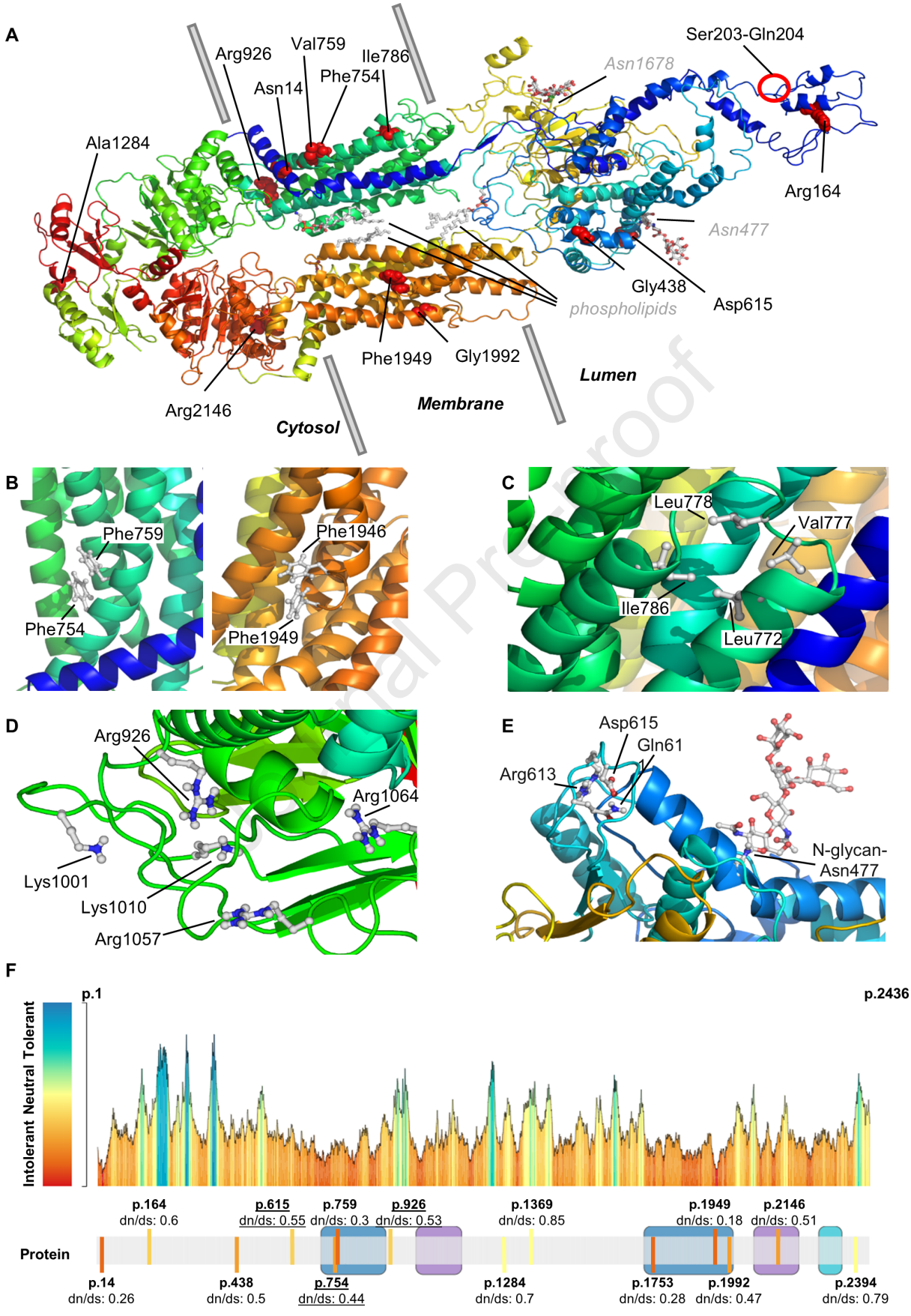
A
Arg926
Val759
Ile786
Phe754
Asn14
Ala1284
Ser203-Gln204
Asn1678
Arg164
Asn477
Gly438
Asp615
phospholipids
Phe1949
Gly1992
Arg2146
Lumen
Membrane
Cytosol
B
Phe759
Phe754
Phe1946
Phe1949
C
Leu778
Val777
Ile786
Leu772
D
Arg926
Arg1064
Lys1001
Lys1010
Arg1057
E
Asp615
Gln61
Arg613
N-glycan-
Asn477
F
p.1
p.2436
Intolerant Neutral Tolerant
p.164
dn/ds: 0.6
p.615
dn/ds: 0.55
p.759
dn/ds: 0.3
p.926
dn/ds: 0.53
p.1369
dn/ds: 0.85
p.1949
dn/ds: 0.18
p.2146
dn/ds: 0.51
Protein
p.14
dn/ds: 0.26
p.438
dn/ds: 0.5
p.754
dn/ds: 0.44
p.1284
dn/ds: 0.7
p.1753
dn/ds: 0.28
p.1992
dn/ds: 0.47
p.2394
dn/ds: 0.79

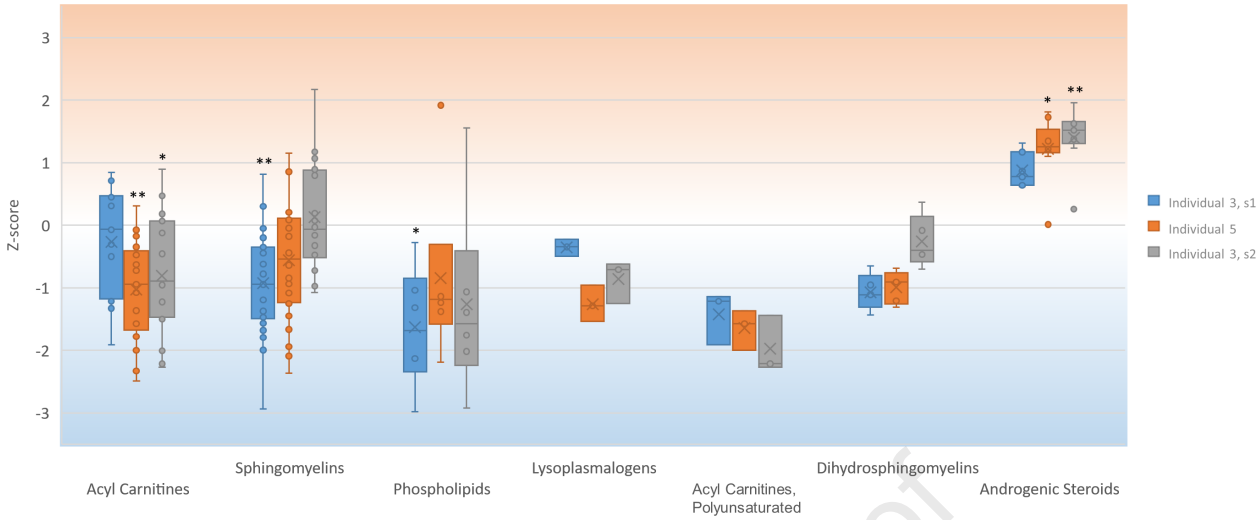

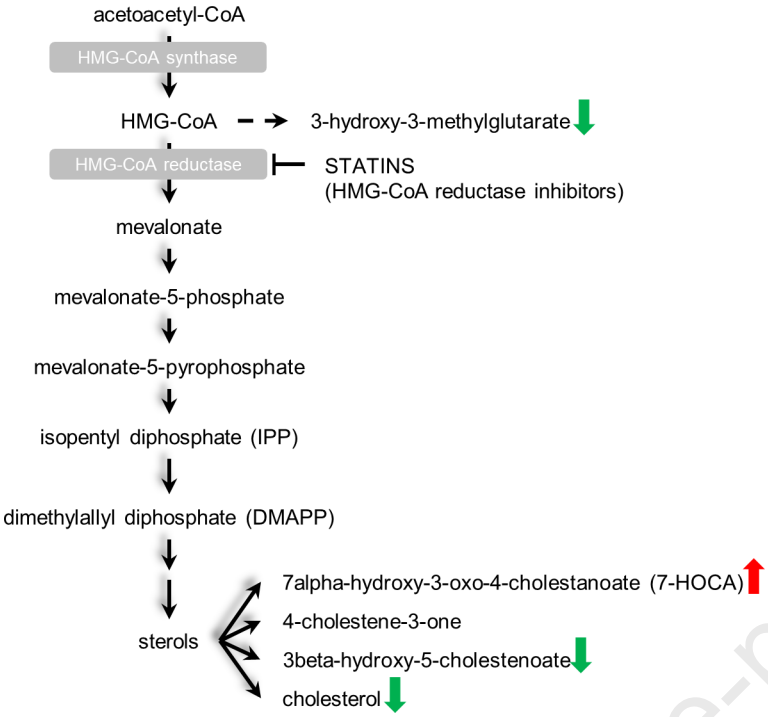

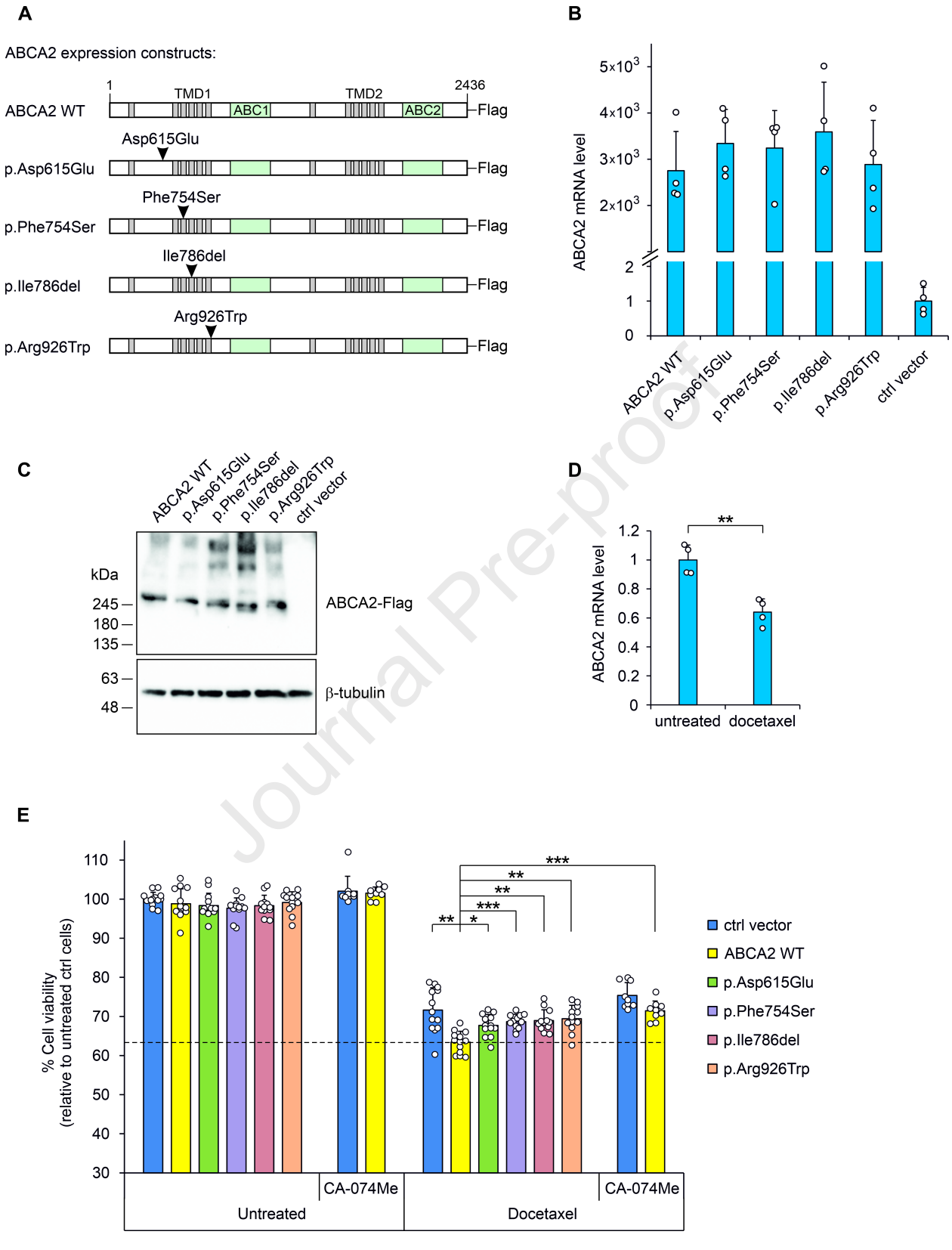

A study describing 17 individuals with mono- or biallelic variants in the *ABCA2* gene. Different methods were used to assess potential for pathogenicity, including a cell viability assay. The results suggest an altered ABCA2 pump function for all four variants included in the experiment and encourage further study of ABCA2.